**ROMANIAN JOURNAL OF INFORMATION SCIENCE AND TECHNOLOGY**
Volume **22**, Number 2, 2019, 103–110

# Analytical modelling of a lateral dual gate MESFET for integrated circuit in SiC

J.F. MOGNIOTTE[1], C. RAYNAUD[2], M. LAZAR[2], and L. MICHEL[2]

[1]Hybria Institute of Business and Technologies, Univ Lyon, INSA Lyon, CNRS, Ampère, F-69621, France
[2]Univ Lyon, INSA Lyon, CNRS, Ampère, F-69621, France
E-mail: jean-francois.mogniotte@insa-lyon.fr, christophe.raynaud@insa-lyon.fr, mihai.lazar@insa-lyon.fr, loic.michel@insa-lyon.fr

**Abstract.** This paper presents a static analytical model derived from a lateral dual gate MESFET in SiC for which the gates have the particularity to be of different physical nature: the first gate is a Schottky barrier and the second gate is a bipolar junction. In order to build a design-kit dedicated to simulation, a spice model has been developed that includes an analytical model of the MESFET which takes into account especially the influence of the both gates on the channel conductivity. The model provides results with a good agreement with experimental measurements and continuous optimization processes allow having a better matching.

**Key-words:** SiC, analytical model, MESFET.

## 1. Introduction

Nowadays, the sector of power electronic changes quickly thanks to the recent introduction of wide band gap devices and particularly of SiC power device (JFET, BJT, MOSFET); such new technological concepts constitute some key points to reduce energy losses. The maturity of the SiC technology allows using these devices in an industrial context to overcome the limits of the current solutions and several technologies (based on SiC MESFET, BJT, MOSFET) have been already manufactured and characterized [1 - 2 - 3]. In this sequel, our research team realized the first step of integrating power circuit technology in SiC based on dual gates MESFET [4 - 5]. This technology is especially designed to be used within power electrical systems dedicated to harsh environment (high temperature ($> 300$ °C) and high voltage ($> 1$ kV)). Despite basic empirical spice-based models have been derived [4] more precise analytical-based models should take into account physical parameters (temperature, carrier mobility…). This paper presents for the first time, the topology of the dual gate MESFET and its working principle. The paper is

structured as follow: the second part presents the principle of the proposed lateral MESFET topology for which the associated analytical model is derived in the third part. The last part deals with the experimental validation of the model in static working conditions. With the independent control of the gates, it confers the possibility to have two degrees of freedom for the control of a circuit. A ring oscillator circuit based on three dual gate MESFETs could be used as Voltage Controlled Oscillator circuit (VCO) with the same design thanks to the biasing of the second gate [5]. Classical solutions for the regulation of power converter as for example the sliding-mode [6 - 7], the dual-gate MESFET allows considering a new way for the design and the control of a power device and new type of circuit in power converters [5 - 8]. To analyze these new topologies, it is necessary to build an analytic model taking into account the influence of the both gates technology. The equations of the model could be implemented in VHDL-AMS and used for simulations of power converters.

## 2. Description of the lateral MESFET

The devices have been manufactured by the CNM-IMB, on a 3 inch semi-insulating 4H-SiC wafer. Details of manufacturing are presented in [4]. A semi-automatic probe station and a Keysight B1505 analyzer have been used for the measurement of the electrical characteristics of lateral dual-gate MESFETs.

a) The topology

Fig.1 presents the typical topology of the device. The MESFET has two layers. The buried P layer has a doping level $N_A$ of $5\times10^{15}$ cm$^{-3}$ and a thickness $H_p$ = 5 $\mu$m. The N layer has a doping level $N_D = 10^{17}$ cm$^{-3}$ and a height $H_n$ = 0.5 $\mu$m. This MESFET is a four terminal device, with 4 metallic contacts named the drain (D), the source (S) and two gates $G_1$ and $G_2$. The first gate $G_1$ is a Schottky contact and the second gate $G_2$ is a bipolar contact (ohmic contact on the buried layer creating a junction-FET with the lateral channel). The buried gate contact $G_2$ is located in the top of the P layer. It has been chosen to isolate the contact $G_2$ by etch. This lateral MESFET is an innovative topology, which mixes two types of junctions (Schottky and bipolar).

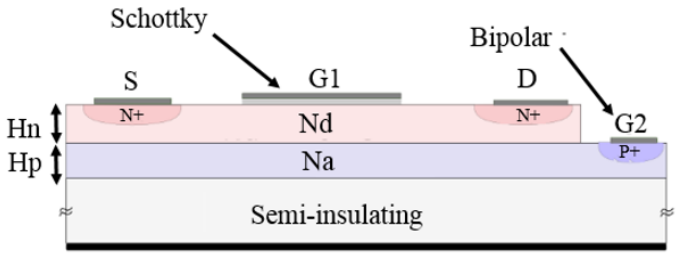


**Fig. 1.** Cross view of the lateral MESFET with the dual gates $G_1$ and $G_2$.

b) Operating principle of this MESFET

In a classical MESFET, there is no second gate $G_2$ and the flow of the current from source to drain $I_{DS}$ is controlled by the extension of a Space Charge region (SCR) under the gate $G_1$. For a given voltage between source and gate called the threshold voltage $V_{TH}$, the SCR width equals the thickness $H_n$, then no more current is passing and the transistor is blocked. The width of the

SCR is given by

$$W_1(x) = \sqrt{\frac{2.\varepsilon.(V_{bi1} - V_{GS1} + \psi(x))}{q.N_D}} \tag{1}$$

where $V_{\text{bi1}}$ is the built-in potential of the Schottky diode $G_1$, and therefore related to the Schottky barrier height of $G_1$, $V_{\text{GS1}}$ is the gate to source voltage, $\Psi(x)$ the potential in the n-layer, x the lateral coordinates from the source (x = 0) to the drain (x = L). Other parameters are defined in Fig. 1 and Table 1. For a classical Schottky barrier (nickel) on n-type 4H-SiC, the barrier height is in the 0.7 eV range.

In our dual gate MESFET, the presence of the bipolar junction involves a second SCR, that extends from the buried junction. The width is given by an expression similar to (1):

$$W_2(x) = \sqrt{\frac{2.\varepsilon.(V_{bi2} - V_{GS2} + \psi(x))(N_A + N_D)}{q.N_A.N_D}} \tag{2}$$

where $V_{\text{GS2}}$ is the gate ($G_2$) to source voltage, $V_{\text{bi2}}$ is the built-in potential of the bipolar junction (for 4H-SiC ∼2.7 eV), given by :

$$V_{bi2} = \frac{kT}{q} ln\left(\frac{N_A.N_D}{n_i^2}\right) \tag{3}$$

$n_i$ is the intrinsic carrier concentration, and k the Boltzmann's constant. It is therefore possible to control the current flow also by biasing $G_2$ (negatively with respect to the source in this case), or by simultaneous biasing of $G_1$ and $G_2$. Fig. 2 presents the cross view of the dual gate MESFET, when both gates are negatively biased (in reverse regime). In this configuration, the two SCR extend, from each side of the conducting n-layer. The dual-gate MESFET is an innovative SiC technology, which allows to modulate with two degrees of freedom the current through the channel of the device and to consider new ways of control.

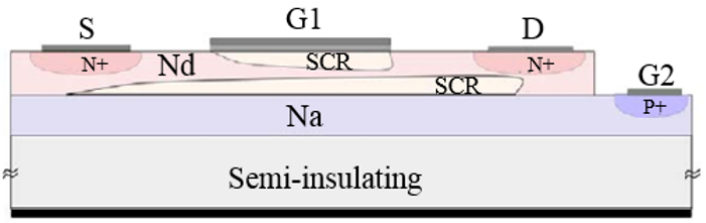


**Fig. 2.** Cross view of a lateral MESFET controlled by the gates $G_1$ and $G_2$.

**Table 1.** Parameters extracted from the experimental measurements of the $I_{DS}$ = f($V_{GiS}$) for $V_{GiS}$ = –5 V (i = "1", "2" or "1–2") and $V_{DS}$ = 20 V

| Configuration of the gate(s) | G1 | G2 | G1−2 |
|---|---|---|---|
| Transconductance (mS) | 2 | 6.8 | 1.2 |
| Transconductance by unit of length (mS/mm) | 5 | 17 | 3 |
| Threshold voltage $V_{TH}$ (V) | $-9$ | $< -40$ | $-7$ |

# 3. Established model of the dual-gate MESFET

The proposed model is based on the dual gate JFET model proposed by H. Morel [9]. In the linear mode, and assuming that the current is only a drift current and is only depending on x, the current across the channel of the device is given by:

$$i_{CH} = q.\mu_D.N_D.A_{CH}(x).\frac{d\Psi}{dx} \tag{4}$$

with $\mu_D$ the electron mobility in the channel, assumed to be uniform in the channel, and $A_{CH}(x)$, the section of the channel expressed as :

$$A_{CH}(x) = Z.(H_n - W_1(x) - W_2(x)) \tag{5}$$

Defining the voltage

$$V_p = \frac{q.N_D.(H_n)^2}{2.\varepsilon} \tag{6}$$

allow to express $i_{CH}$ as

$$\int_0^L i_{CH}.dx = Z.q.N_D.\mu_D.H_n \int_0^{V_{CH}} \left(1 - \frac{W_1(x)}{H_n} - \frac{W_2(x)}{H_n}\right).d\Psi \tag{7}$$

Where $V_{CH}$ is the voltage drop along the channel.
After integration,

$$i_{CH} = \frac{V_{ch}}{R_{CH}}(\upsilon - \frac{2}{3}.(\upsilon+\gamma_1)^{\frac{3}{2}} + \frac{2}{3}.(\gamma_1)^{\frac{3}{2}} - \frac{2}{3}.\frac{1}{\sqrt{\alpha}}.(\upsilon+\gamma_2)^{\frac{3}{2}} + \frac{2}{3}.\frac{1}{\sqrt{\alpha}}.(\gamma_2)^{\frac{3}{2}} \tag{8}$$

where

$$\upsilon = \frac{V_{CH}}{V_P}, \gamma_1 = \frac{V_{bi1} - V_{GS1}}{V_P}, \gamma_2 = \frac{V_{bi2} - V_{GS2}}{V_P}, \alpha = \frac{N_A}{N_A + N_D} \text{ and } R_{CH} = \frac{L}{Z.q.N_D.\mu_D.H_n}$$

The channel is blocked when $W_1(x)$+$W_2(x)$=$H_n$, so when

$$\sqrt{\upsilon+\gamma_1} + \frac{\sqrt{\upsilon+\gamma_2}}{\sqrt{V_P.\alpha}} = 1 \tag{9}$$

We define now

$$X = \sqrt{\upsilon+\gamma_1} \tag{10}$$

so that the channel is blocked when

$$X^2\left(\frac{1-\alpha}{\alpha}\right) + 2X + \frac{\gamma_2 - \gamma_1 - \alpha}{\alpha} = 0 \tag{11}$$

Resolving (11) allows determining the value of v for which the channel is blocked.

$$v_1 = (X_1)^2 - \gamma_1 \tag{12}$$

$$v_2 = (X_2)^2 - \gamma_1 \tag{13}$$

where $X_1$ and $X_2$ are the solution of (11). Therefore in the linear operation mode (v $<$v $_2$), the current in the channel is given by (8), when v $\geq$ $v_2$, the current is given by (8) using v = $v_2$. Moreover, taking into account the different series resistances, the drain to source voltage $V_{ds}$ is given by:

$$V_{ds} = R_S.i_{ds} + V_{CH} \tag{14}$$

where $R_s$ is the total series resistance.

**Table 2.** Synthesis of the parameters use for the analytical model

| Name | Definition | Units |
|---|---|---|
| q | elementary charge | C |
| $N_D$ | Doping concentration in the channel | $cm^{-3}$ |
| $V_{CH}$ | Voltage at terminals of the channel | V |
| $\mu_D$ | electron mobility | $cm^2.V^1.s^{-1}$ |
| $W_1(x)$ | space charge region for the Schottky junction | cm |
| $W_2(x)$ | space charge region for the bipolar junction | cm |
| $H_n$ | thickness for the channel of the device | cm |
| Z | width of the channel | cm |
| L | length of the channel | cm |
| $V_{bi1}$ | internal potential of the Schottky junction | V |
| $V_{bi2}$ | internal potential of the bipolar junction | V |

# 4. Experimental results

This simple analytical model is compared with the experimental data. In all following theoretical calculations, the parameters for which the best fit is reached are: $H_n$ = 0.53 $\mu$m, $N_D = 1.14\times10^{17}$ $cm^{-3}$ and $N_A = 5\times10^{16}$ $cm^{-3}$. They are in very good agreement with technological values. The geometrical parameters are Z = 440 $\mu$m and L = 20 $\mu$m.

The MESFETs have been characterized in the ON mode for three configurations: polarization of $G_1$ with floating $G_2$, polarization $G_2$ with floating $G_1$ and polarization of $G_1$–$G_2$ with the same value. Fig. 3 presents the static characteristics $I_{DS}$=f($V_{DS}$) that includes a bias applied both on $G_1$ and $G_2$. The device presents the expected behavior. The MESFET is ON, when 0 V is applied on the gates. The value of the current is reduced, when a decreasing negative voltage is applied on both gates until the MESFET is turned off. The device is blocked at $V_{G1S}$ = – 10 V. On the experimental data are superimposed the theoretical characteristics calculated with the model previously detailed. Global shapes of the curves are similar, showing a limit between the linear regime and saturated regime coherent with the data.

For lower $V_{GS}$ values, theoretical currents are lower than experimental ones, although they remain in the same range. The difference can be explained by the assumptions made in the analytical model (take into account more physical laws) and by the technological process of the device (eg: contact resistor with high value), which limit the electrical performance of the MESFETs [4]. Fig. 4 compares experimental and theoretical data in the case of $G_2$ floating. For numerical calculations, $V_{G2}$ has been set to 0. Agreement is not as good as in the case $G_2$ is bias as $G_1$, probably due to a floating bias that makes $V_{G2} \neq 0$.

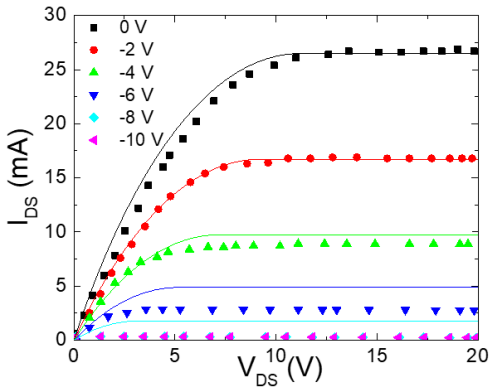


**Fig. 3.** Comparison between the analytical model (dots) and the measurement (lines) of the MESFET for $I_{DS}$ =f ($V_{DS}$) with $V_{GS1}$ = $V_{GS2}$.

Study of the effect off-polarization of floating gate can be due on the transconductance curves. Fig. 5 shows $I_{DS}$ = f($V_{GS}$) measured in different cases (floating $G_1$, floating $G_2$, and short circuit between $G_1$ and $G_2$). From the experimental measurements, it appears that the bias of the buried P layer slightly influences the current in the channel. The $I_{DS}$ current changes from 41 mA with $V_{G2S}$ = 0 V to 23 mA with $V_{GS2S}$ = –20 V. The Table 1 synthesizes the extracted value of the transconductance and the threshold voltage for each configuration. The 3rd configuration (short-circuit between $G_1$ and $G_2$) is the best, the transconductance presents the lower value in this case (1.2 mS, see Table 1). In this configuration, the gates $G_1$ and $G_2$ are at the same value. From the experimental results, only the gate G1 can block entirely the MESFET. The gate $G_2$ allows only modulating the current through the lateral channel for these devices. Numerical calculations fit rather well the experimental data except when $G_1$ is floating. When $G_1$ is floating, calculations with $V_{GS1}$ = 0 does not match the experimental data. Assuming that $G_1$ is influenced by the bias of $G_2$, such as $V_{GS1} = 0.05 \times V_{GS2} + 1.8$, gives a very good fit of the transconductance curve.

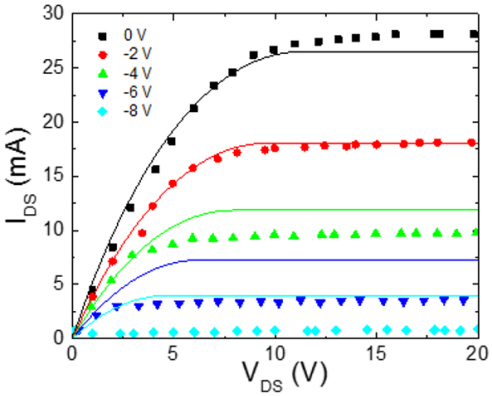


**Fig. 4.** Comparison of $I_{DS}$ =f ($V_{DS}$) curves between the analytical model (dots) and the measurement (lines) of the MESFET with $V_{GS2}$ = 0 V in theoretical curves and $V_{G2}$ is floating in experimental ones.

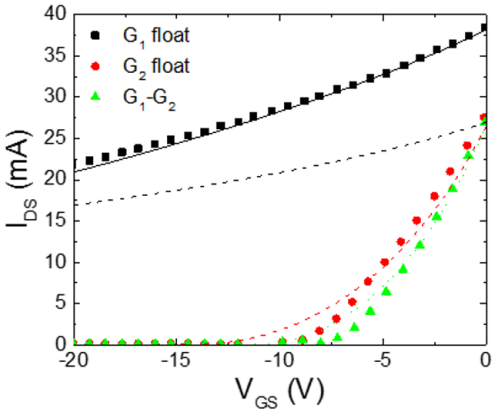


**Fig. 5.** Comparison of the experimental transconductances $I_{DS} = f(V_{GiS})$ of a dual-gates MESFET for $V_{DS}$=20 V (symbol) in the 3 cases: $G_1$ is floating, $G_2$ is floating, and $V_{G1} = V_{G2}$. Dash line corresponds to numerical simulations. The solid line is calculated using $V_{GS1} = 0.05 \times V_{GS2} + 1.8$.

## 5. Conclusion

A dual-gate MESFET device has been presented, which consists in both a Schottky junction and a bipolar junction. It is therefore possible to control the MESFET by either the gate $G_1$, or the gate $G_2$ or the both. The dual gate structure of the power switch allows considering several working modes such as linear control or bang-bang control. Potential applications include high current pulse generators that generate specific shaped signals where the MESFETs work in linear mode. However, in order to design circuits based on the proposed device, it is necessary to take into account the modulation of the channel by the dual-gate. An analytical model of the MESFET has been developed and confronted to experimental data. The model fits with the experimental data in nearly all cases. A more difficult aspect is to predict the current when the Schottky gate is floating. Experimental data do not match with the model without assuming that the Schottky gate is biased under the influence of the second gate. This model can be used in mixed-mode simulation but further improvements are needed to examine how and why the potential of the floating gate can be controlled.

**Acknowledgements.**Thanks are due to the National Center of microelectronics of Barcelone (CNM) of the Institute of Microelectronics of Barcelona (IMB) for manufacturing the devices and to the “Direction Générale de l’Armement” (DGA) for its financial support.

## References

[1] KARGARRAZI S., LANNI L., RUQC A., ZETTERLING C. M., *A monolithic SiC drive circuit for SiC Power BJTs*, Power Semiconductor Devices & IC’ (ISPSD), 2015 IEEE 27th International on May 2015, Hong Kong (China), pp. 285–288.

[2] ALEXANDRU M., BANU V., JORDA X., MONTSARRAT J., VELLVEHI M., TOURNIER D., MILLAN J., GODIGNON P., *SiC Integrated Circuit Control Electronics for High-Temperature Operation*, IEEE Transactions on Industrial Electronics, **62**(5), 2015, pp. 3182–3191.

[3] KUHNS N., CALEY L., RAHMAN A., AHMED S., DI J., MANTOOTH H. A., FRANCIS A. M., HOLMS J., *Complex High- Temperature CMOS Silicon Carbide Digital Circuits Designs*, IEEE Transactions on Device and Materials Reliability,**16**(2), June 2016, pp. 105–111.

[4] MOGNIOTTE J. F., TOURNIER D., RAYNAUD C., LAZAR M., PLANSON D., ALLARD D., *Silicon Carbide technology of MESFETs-based power integrated circuits*, Journal of Emerging and Selected Topics in Power Electronics (JSTPE), **6**(2) 2018, pp. 539–548.

[5] MOGNIOTTE J. F., RAYNAUD C., LAZAR M., PLANSON D., ALLARD D., *SiC integrated circuits for smart power converter*, Romanian Journal for Information Science and Technology, **20**(4) 2017, pp 385–399.

[6] YAN W., HU J., UTKIN V., *Sliding mode pulsewidth modulation*, IEEE Transaction on Power Electronics, **23**(2), 2008, pp 619–626.

[7] LEON-MASICH A., VALDERRAMA-BLAVI H., BOSQUE-MONCUSI J. M., MAIXE-ALTES J., MATERNIEZ-SALAMERO L., *Sliding mode control based boost converter for high Voltage low power applications*, IEEE Transactions on Industrial Electronics, **62**(1), 2015, pp 229–237.

[8] MOGNIOTTE J. F., TOURNIER D., PLANSON D., BEVILACQUA P., GODIGNON P., *Design of an integrated power converter in Wide Band Gap for harsh environments*, 7th Conference on Integrated Power Electronics Systems (CIPS), Nuremberg (Germany), pp. 1–6, March 2012.

[9] MOREL H., HAMIEH Y., TOURNIER D., ROBUTEL R., DUBOIS F., RISALETTO D, MARTIN C., BERGOGNE D., BUTTAY C., MEURET R., *A multi-Physics Model of the VJFET with a lateral channel*, 14th European Conference On Power Electronics and Applications (APEC), Birmingham (UK), September 2011.